JOURNAL OF THE ROYAL SOCIETY Interface

*J. R. Soc. Interface* (2012) **9**, 640–647
doi:10.1098/rsif.2011.0395
*Published online* 24 August 2011

# Tilted cellulose arrangement as a novel mechanism for hygroscopic coiling in the stork's bill awn

**Yael Abraham[1,2], Carmen Tamburu[3], Eugenia Klein[4], John W. C. Dunlop[2], Peter Fratzl[2], Uri Raviv[3] and Rivka Elbaum[1,*]**

[1]*The Robert H. Smith Institute of Plant Sciences and Genetics in Agriculture, The Hebrew University of Jerusalem, Rehovot 76100, Israel*
[2]*Department of Biomaterials, Max Planck Institute of Colloids and Interfaces, Potsdam-Golm 14424, Germany*
[3]*The Institute of Chemistry, The Hebrew University of Jerusalem, Edmond J. Safra Campus, Givat Ram 91904, Israel*
[4]*The Department of Chemical Research Support, The Weizmann Institute of Science, Rehovot 76100, Israel*

The sessile nature of plants demands the development of seed-dispersal mechanisms to establish new growing loci. Dispersal strategies of many species involve drying of the dispersal unit, which induces directed contraction and movement based on changing environmental humidity. The majority of researched hygroscopic dispersal mechanisms are based on a bilayered structure. Here, we investigate the motility of the stork's bill (*Erodium*) seeds that relies on the tightening and loosening of a helical awn to propel itself across the surface into a safe germination place. We show that this movement is based on a specialized single layer consisting of a mechanically uniform tissue. A cell wall structure with cellulose microfibrils arranged in an unusually tilted helix causes each cell to spiral. These cells generate a macroscopic coil by spiralling collectively. A simple model made from a thread embedded in an isotropic foam matrix shows that this cellulose arrangement is indeed sufficient to induce the spiralling of the cells.

**Keywords: hygroscopic movement; coiling; cellulose; microfibril angle; small-angle X-ray scattering; *Erodium***

## 1. INTRODUCTION

Seeds enable the spread of plants to new locations and their survival through harsh periods [1]. Dispersion requires various mechanisms, often-involving animals, wind or water, combined with soil movements [2]. In many cases, the seed-dispersal unit develops a dehiscence tissue, which is a specialized tissue that enables the seed to separate from the mother plant [3]. After disconnecting, the tissue attached to the seed desiccates and dies. However, it can still direct the seed to a safe germination place through specific morphologies that interact with the environment. These structures may be wing-like appendages attached to maple and pine seeds, parachutes attached to dandelion and milkweed seeds, low-density tissue facilitating water dispersal of coconuts, spikes and adhesives to attach to animals in burdock and alfalfa and so on (examples in [2–4]). Some seeds, such as the wheat awn [5], pinecones [6] and wild carrot [7], are dispersed by the action of elaborate multi-celled organs that generate movement via changes in the hydration of the cell walls. Even seedless plants use hygroscopic apparatuses to disperse spores. These include the annulus of leptosporangiate ferns [8] and the elaters of *Equisetum* [9] and some liverworts [10]. As metabolically inactive tissues, the hygroscopic dispersal apparatuses are well suited to inspire biomimetic objects [11].

Dead plant tissues consist mainly of cell walls that can be regarded as a composite material built primarily of crystalline cellulose microfibrils, embedded in a soft matrix of polysaccharides, aromatic compounds and structural proteins. The tough construction performs as a load-bearing element in the plant tissue and is capable of withstanding cell turgor pressure [12]. The cell wall controls the complex shape of plants [13] and their mechanical behaviour [14]. The juxtaposition of plant cells with different mechanical properties may induce stress or movement (or both), when one region of the tissue contracts (or expands), whereas the adjacent cells do not. This results in accumulation of tension in the tissue. The tension may relax to create deformation (movement) of the tissue [15]. In drying tissues, the direction of the contraction reflects the cellulose microfibril orientation: When the cell wall dries, the matrix

*Author for correspondence (elbaum@agri.huji.ac.il).

Electronic supplementary material is available at http://dx.doi.org/10.1098/rsif.2011.0395 or via http://rsif.royalsocietypublishing.org.

*Received* 20 June 2011
*Accepted* 1 August 2011

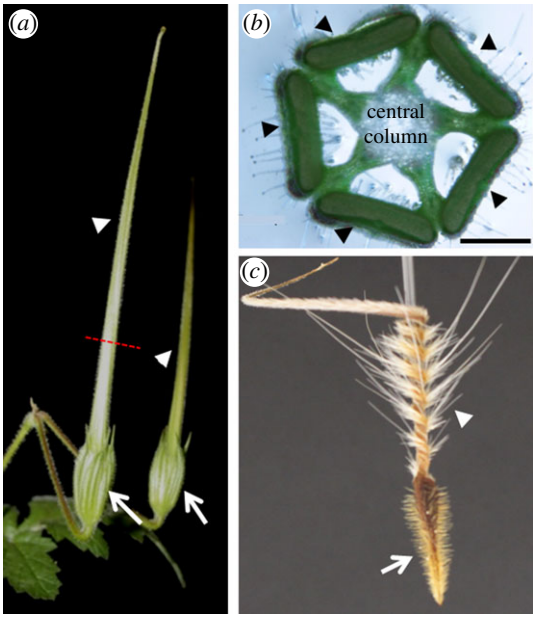


Figure 1. The morphology of the fruit of stork's bill (*Erodium gruinum*). (*a*) Two complete stork's bill-shaped fruits, about 4 days prior to ripening. Arrows indicate the location of the seed; arrowheads indicate the awns. Dashed red line indicates the part from which cross section (*b*) was taken. (*b*) *Erodium gruinum* fruit in cross section depicts five awns (indicated by arrowheads) connected by a central column. (*c*) Dry awned seed showing the coiling region (arrowhead) close to the seed (arrow). Scale bar, (*b*) 1 mm.

between the microfibrils shrinks while the crystalline microfibrils do not, as they do not incorporate water. Therefore, the cell wall contracts in a direction essentially perpendicular to the microfibril orientation. The contraction increases with the angle between the microfibrils and the long axis of the cell, the microfibril angle (MFA) [16].

Hygroscopic plant tissues may consist of two basic layers that differ in the organization of their cellulose fibrils, and therefore in their contraction properties [17–20]. Bending actuators are formed when cells with a low MFA resist the contraction of drying cells with high MFAs. Two other types of deformation may appear in hygroscopic dispersal mechanisms: a twist around the long axis of the unit, and a coil, in which the long axis of the unit is twisted and bent to create a helical spring. Mechanical models and theoretical analysis show that a band, consisting of two layers that contract in opposite directions, forms a bend, coil or twist simply by rotating the directions of the contractions in relation to the long axis of the band [21]. Contrary to this, we found that the coiling in stork's bill (*Erodium gruinum*) dispersal units requires only a single layer with a uniform microfibril arrangement.

The stork's bill fruit consists of five seeds equipped with long tapering appendages (awns) attached to a central column (figure 1). The awns display hygroscopic coiling movement during fruit drying. Thus, tension accumulates as the awns are prevented from coiling by their attachment to the central column. The tension increases until the dehiscence tissue snaps, and the seed-dispersal units are flung from the parent plant [22]. This movement is based on a bilayer structure, consisting of the contraction of the awn against the central column. Once on the ground, the coiled awns (figure 1*c*) respond to the diurnal humidity cycle and propel the seeds across the ground and into the soil [23,24]. Herein, we reveal the structural hygroscopic mechanism in these awns. Unlike the common bilayered structures, the stork's bill awn itself exhibits a coiling movement that originates from a mechanically uniform cell layer made up of intrinsically coiling cells.

## 2. CELLULOSE ORGANIZATION IN THE STORK'S BILL AWN

We examined the coiling region of the awns by electron and light microscopy. Cross sections reveal a layered structure, when each homogeneous layer is characterized by a typical cell wall morphology (figure 2). Similar to other hygroscopically active tissues, we distinguish between a thick layer that faces into the coil ('the inner layer') and a narrow layer that faces outwards from the coil ('the outer layer'; figure 2*a,d*). On the fruit, the inner layer is distal to the central column. The two layers are connected by cells with thin cell walls. Scanning electron micrographs obtained from a fractured awn revealed cellulose microfibrils, which appear to wind around the cell, at an angle close to 90° in the inner layer (figure 2*c*). The outer layer (figure 2*b*) displays smoother break morphology consistent with microfibrils running perpendicular to the fracture [26]. Polarized light microscopy showed similar tendencies (figure 2*d,e*).

To our surprise, when we split the awn lengthwise to separate between the inner and the outer layers, we found that the inner layer coils even more tightly than the complete awn (the complete awn had five to six coils, whereas the isolated inner layer had seven to eight; figure 3*a,b*). The separated outer layer slightly curves and coils towards the inner layer, in the same coiling direction as the complete awn. In addition, thin longitudinal strips of the inner layer were also found to coil (figure 3*c,d* and electronic supplementary material, video S1), as do mechanically separated single cells (figure 3*e*). This single homogeneous coiling layer rules out the ubiquitous bilayer model, and leads us to conclude that the coiling of the stork's bill awn stems from an intrinsic property of the cells in the inner layer. Single cells (about 1 mm long and 15 μm wide) cooperate to produce a macroscopic coil. As the awn dries, its main longitudinal axis is bending and twisting at the same time (electronic supplementary material, video S2). This distortion is manifested as coiling of the entire bundle of cells.

The cellulose microfibril orientation in the isolated inner layer was measured by X-ray scattering. Using an in-house set up [27], small-angle X-ray scattering (SAXS) patterns were obtained by irradiating samples of about 200 μm thick (approx. 20 cell layers). The samples were positioned with the awn's longitudinal axis in vertical direction, perpendicular to the X-ray beam. Unusual patterns were obtained that consisted of a single streak with a clockwise tilt in relation to

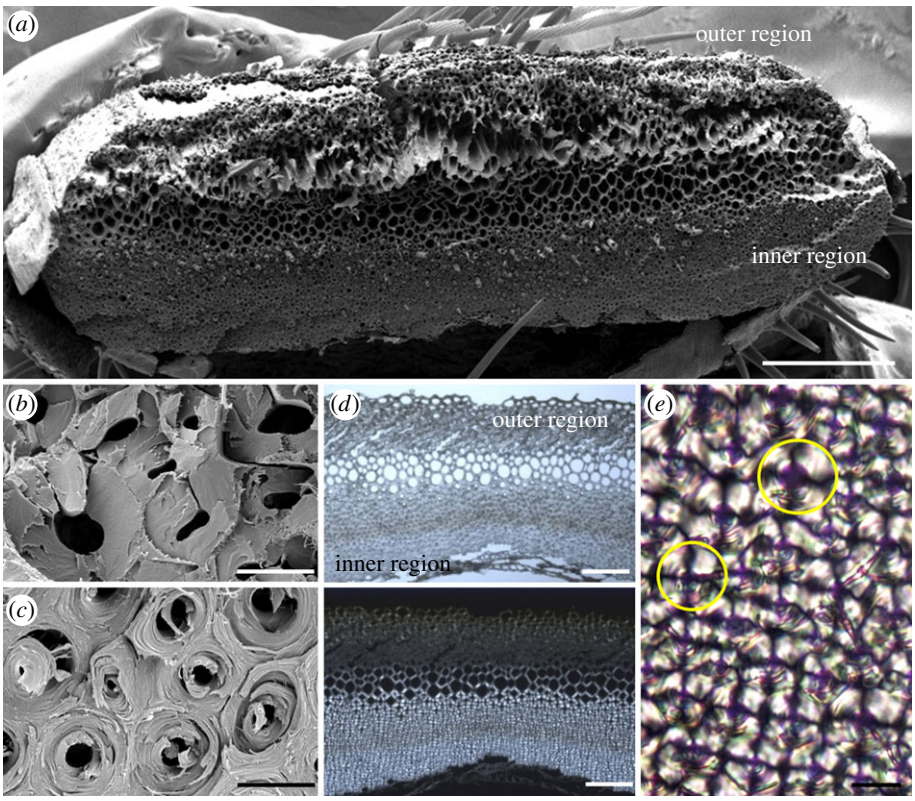


Figure 2. Microscopic images of the awn cross section at the coiling region. (*a*) Overview of a fractured cross section taken by scanning electron microscope. (*b*) A close up of the coil outer layer reveals a brittle break morphology. (*c*) A close up of the inner layer reveals spool-like packing of the cellulose fibrils, which is typical of the whole layer. (*d*) Light (upper panel) and polarized light (lower panel) microscopy images of a 10 µm thick cross section from the coiling region of the awn. Under crossed polarizers, the part facing the inner side of the coil is brighter, indicating a relatively high microfibril angle. (*e*) A close up of the cells in the inner layer, revealing a dark cross which is typical of circular birefringent materials (such as starch granules [25]). Yellow circles delineate the margins of a cell. Scale bars, (*a*) 250 µm, (*b*,*c*,*e*) 10 µm and (*d*) 100 µm.

the meridian, starting at about 20° tilt at the bottom of the coiling region to about 10° at its top (figure 4*a*). In addition, when the sample was rotated by 180° around its long axis, a mirror image of the original scattering pattern was obtained. Typically, common elongated cells in which the cellulose fibrils are wound in a helix around the cell (figure 5*a*) show fan-shaped SAXS patterns, symmetrical around the equator and the meridian [28]. The fact that the inner layer showed only a single narrow streak indicates that the cellulose microfibrils are wound around the cell in a helix with a very small pitch. More importantly, the tilt of the streak indicates a tilted orientation of the microfibrils in relation to the awn's long axis. Thus, two possible structural configurations may be inferred—a tilted arrangement of the cells themselves with respect to the awn axis (with a cellulose MFA of 90°), or a tilted helix arrangement of the cellulose microfibrils within the cell wall (figure 5*b*). Nevertheless, longitudinal sections show that the stork's bill awn cells are in fact aligned parallel to the awn axis (figure 4*b*), which excludes the first option. In support of the second option, cryo-scanning electron images of single cells show cellulose fibrils winding around each cell to create a very tightly wound tilted helix (figure 4*c*). The clear single streak in the SAXS patterns implies that the cellulose tiling direction is uniform in all cells, with similar slopes on the proximal and distal sides of the cells, and a slope change at the lateral sides (figure 5*c*). This arrangement facilitates the cooperative way by which the cells induce the macroscopic coiling of the awn.

## 3. COILING MECHANISM

Single cells from the inner layer coil when they dry, as the cell wall matrix contracts against the cellulose microfibril scaffold. Our hypothesis is that the stress applied to the tilted cellulose helices induces coiling of the whole cell. To test this, we created a model of a cell made of a polyurethane sponge in the shape of a long rectangular cylinder. The cylinder is wound tightly by a thin non-extendable thread that was sewn into the sponge at the corners as a normal or a tilted helix (figure 6*a*,*b*). The tightening of the thread compresses the isotropic matrix of the sponge in directions that are set by the helix scaffold. The helical scaffold experiences expansion forces that induce a deformation of the whole structure, similar (but opposite) to the contraction forces, which are experienced by the cellulose scaffold in the awn cells. The extent of the deformation depends on the geometry of the helix and the level of expansion (compression). A scaffold of a normal (non-tilted) helix induces twisting of the cylinder around its own axis, in a twist direction opposite to that of the helical thread (figure 6*e*,*f*). Indeed, microscopic twisting response to

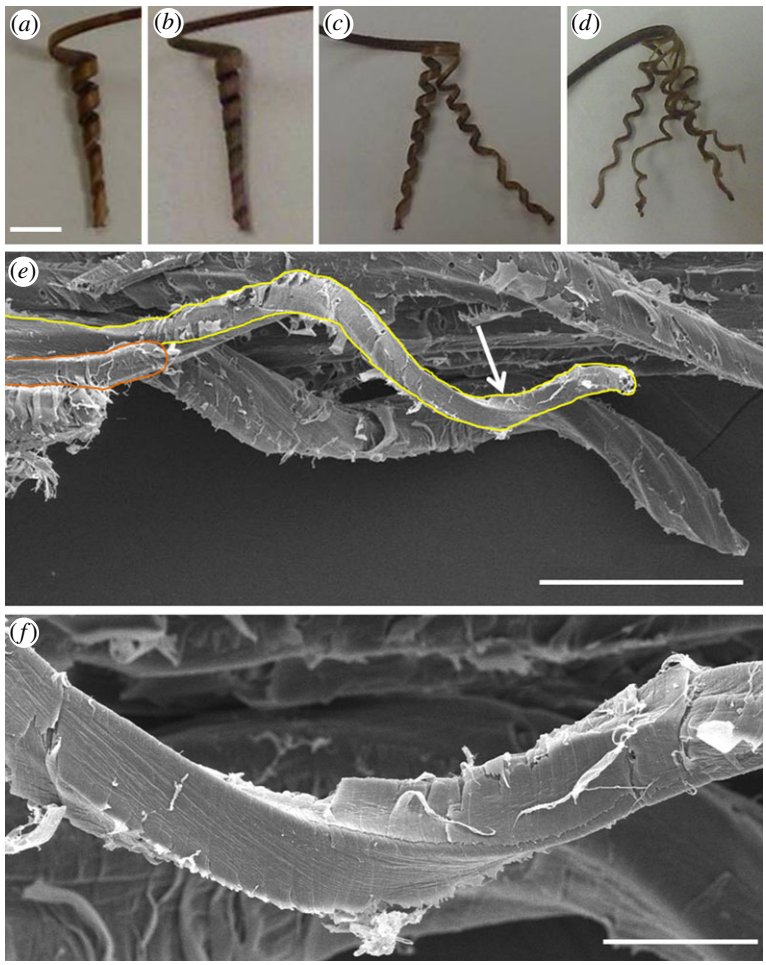


Figure 3. Cooperative cell spiralling creates the macroscopic coil. (*a*) The coiling section of the complete awn showing five to six coils. (*b*) The separated inner layer of the awn, showing seven to eight coils. The inner layer, split into (*c*) once and (*d*) twice still coils to about the same extent as the complete inner layer (the distortions of some of the sections result from the unevenness of the cuts). (*e*) Scanning electron micrograph of the inner layer of the awn showing a group of coiling cells behind a single coiled cell connected to the tissue at one end (delineated). (*f*) A close up of the cell region is indicated by an arrow in (*e*). Scale bars, (*a*–*d*) 5 mm, (*e*) 100 µm and (*f*) 20 µm.

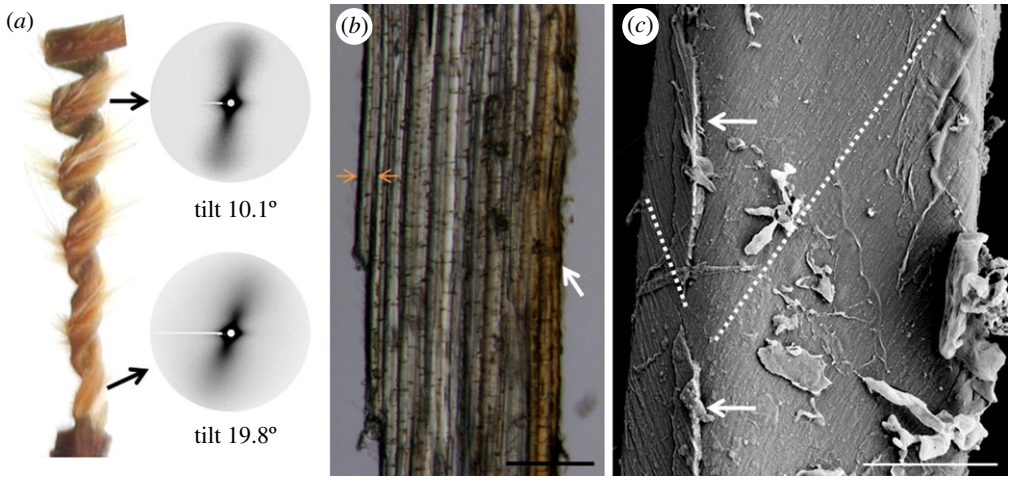


Figure 4. The cellulose microfibrils organization in the cell walls of the coiling cells. (*a*) Small-angle X-ray scattering (SAXS) pattern of a vertical sample from the inner layer of the stork's bill awn, measured at the top and bottom parts of the coiling region. The tighter coil in the bottom part shows a larger SAXS tilt. (*b*) Longitudinal section of the inner layer showing the cells' alignment with the length of the awn. As the length of single cells is about 1 mm, it is impossible to see complete cells in this view. (*c*) Cryo-scanning electron image showing the change in microfibril angle in a single cell, marked by a broken line. Arrows indicate remains of the middle lamella. Scale bars, (*b*) 100 µm, and (*c*) 5 µm.

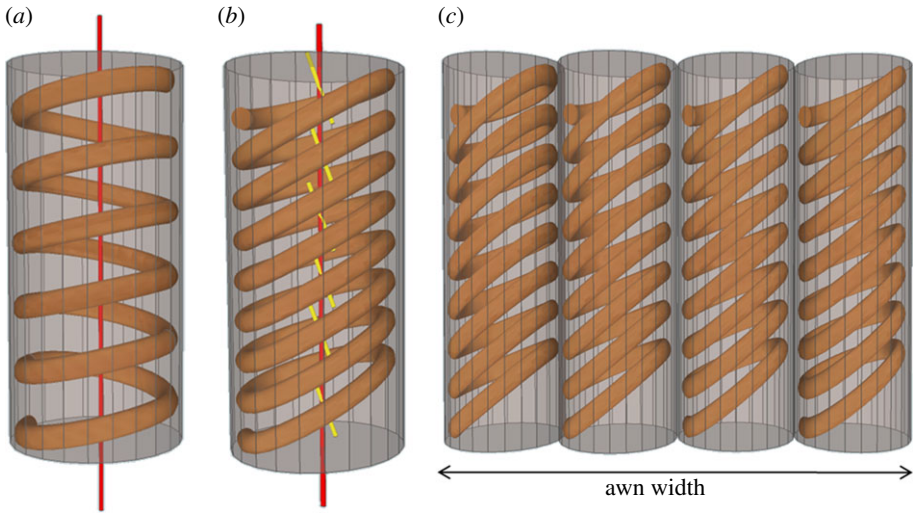


Figure 5. Schematic showing the arrangement of cellulose microfibril in a normal helix (*a*) common in elongated plant cell, compared with a tilted helical arrangement of the cellulose microfibrils in the coiling cells of the stork's bill awn (*b*). In the common plant cell, the cell axis (in red) coincides with the cellulose helix, so that the microfibril angle (MFA) between the cellulose and the cell axis does not change with the circumference of the cell. On the other hand, in the spiralling cells of the stork's bill, the helix axis (in yellow) is at an angle to the cell axis (in red), resulting in the changing of the MFA around the cell. (*c*) A scheme illustrating the identical cell polarity in the inner layer of the awn at the coiling region. The direction of the tilting of the cellulose helix is the same in the cells, with the largest microfibril angle facing towards the wide side of the awn.

cellulose helical scaffold was observed in stressed wood cells [29]. On the other hand, when the sewn helix was tilted, the tightened structure bent in addition to twisting to form a coil (figure 6*a–d*). This confirms that a tilted helix scaffold that confines an expandable matrix will result in the coiling of the construct.

To infer the direction of the cellulose helix in the awns, we noted that the awns and the single cells in the inner layer coil anticlockwise as the cell wall matrix dry and contract (figures 1 and 2; and electronic supplementary material, videos S1 and S2). The model of an expanding matrix (the sponge), constricted by a stiff helical scaffold (the thread), twists and coils in response to an *expansion* force exerted by the sponge matrix on the stiff scaffold. We infer from this that the *contraction* force exerted by the drying matrix in the awn's cell walls induces a similar effect as it shrinks, with a twist induced in the opposite direction. Therefore, the cellulose microfibrils in the cells create a tight anticlockwise helix in agreement with previous observations in wood cells [29,30]. The radius of the coiling sponge varied inversely with the tilt angle of the thread helix (figure 6*c,d*). This is in agreement with the SAXS patterns obtained from along the coiling region of the awn, showing tight coiling (small coil radius and pitch) at the base of the awn, together with a high cellulose tilt angle of about 20° and looser coiling (larger coil radius and pitch) at the top of the coiling region, with a tilt angle of about 10° (figure 4*a*). Our results show that the handedness and pitch of the coil are controlled by varying the characteristics of the helix scaffold.

## 4. DISCUSSION

The seed-dispersal mechanism of stork's bill uses humidity changes in order to both catapult the seed from the plant and propel it across the ground into a safe germination site [31,32]. On the fruit, the drying awns contract, while the central column resists the dimensional change. The persistent contraction results in catapulting the awned seed. At the ejection moment, the coil is loose, because the awn is a pre-stressed viscoelastic material that will relax to a tight coil over minutes. Looking at the awn proper, the cross section from the coiling region reveals a layered structure. In an attempt to characterize the role of each layer, we discovered that the separated homogeneous inner layer coils on its own, ruling out that the coiling is just owing to a macroscopic bilayer effect based on two layers with different expansion. It was found that coiling may occur in twisting objects if their width exceeds a certain value [33]. However, thin strips and even single cells obtained from the inner layer continued to coil, establishing that this hygroscopic coiling originates from specialized cells. The coiling of the cells is governed by the arrangement of the cellulose microfibrils in tight-sheared helices, as illustrated by the sponge models (figure 6). Similarly, twisting of macroscopic paper sheets has been attributed to the nanometric cellulose fibrils' helical conformation [34].

Apparently, the outer layer plays a role in increasing the rigidity of the awn, and not so much in the coiling itself. The orientation of the cellulose microfibrils is almost parallel to the cell axis. This renders the unripe fruit more rigid and erect. High rigidity of the awn is also necessary later, to propel the seed and bury it in relatively rough and hard ground, as was the case when collected in the aeolianite ('kurkar') hills in Nez Ziona, Israel. In addition, the linear arrangement of the cellulose fibrils may affect the water vapour movement in the hygroscopic tissue [35]. Stiffness and water vapour kinetics are important parameters for the awn to actuate the seed by the diurnal humidity

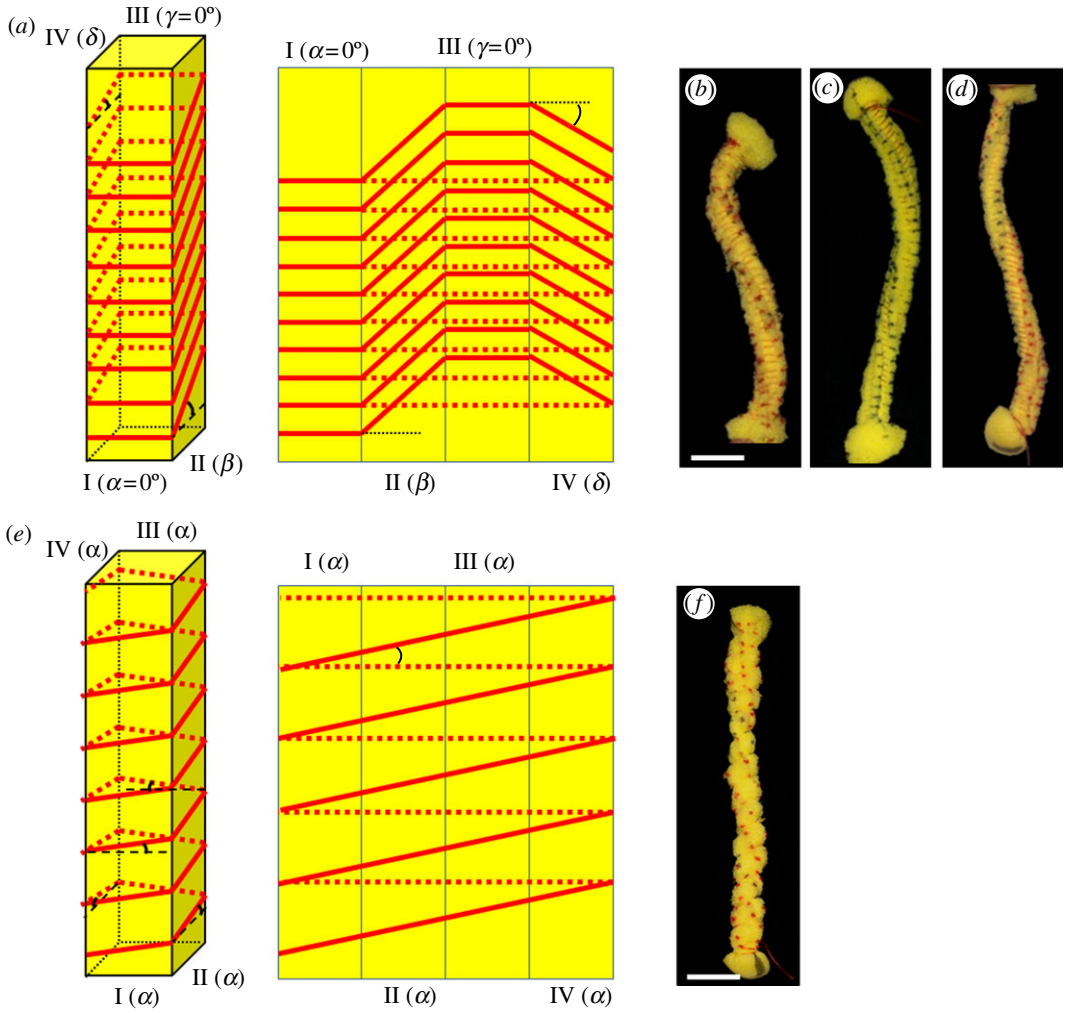


Figure 6. Sponge models simulating the difference in behaviour of drying plant cell walls with normal and tilted helix alignment of the cellulose microfibrils. Long rectangular cylinder sponge strips (approx. $1.5 \times 1.5 \times 12\ \mathrm{cm}^3$) were threaded loosely to form a helix, either tilted (*b*–*d*) or not (*f*). The thread was then tightened, forming a non-extendable cage restricting the expansion of the isotropic matrix of the sponge. (*a*) A scheme (right: three-dimensional, left-sides projections) illustrating the threading angles of the tilted helix models: $\beta$ on side II, and $\delta$ on side IV, whereas sides I and III have $\alpha = \gamma = 0^\circ$. In (*b*) tight anticlockwise thread helix with angles of $\beta = +15^\circ$, $\delta = -8^\circ$ and (*c*) $\beta = +40^\circ$, $\delta = -33.5^\circ$ results in a clockwise coiling of the structure. Note that the coiling radius of the structure is reduced in model (*c*) with the increase in tilt angles. (*d*) For a clockwise thread helix of $\beta = -40^\circ$, and $\delta = +33.5^\circ$, an anticlockwise coil is formed. (*e*) A scheme (right: three-dimensional, left-sides projections) illustrating the threading angles in the normal helix models. All the sides are threaded at the same angle, $\alpha$. (*f*) A normal thread helix with $\alpha = +10^\circ$ produces only a twist with no bending of the structure's longitudinal axis. Scale bar, (*b*–*e*,*f*) 2 cm.

cycles. Together with the slightly coiling tail of the awn and the unidirectional hairs decorating the coiling part (figure 1*c*), the seed-dispersal unit is able to direct the seed to a safe germination site.

In conclusion, the cells in the awn react to water loss by coiling, rather than by twisting that usually appears in normal plant cells [30,36]. Looking for other examples of coiling cells, unexplained cooperative cell coiling was observed in the *Arabidopsis* mutant *tortifolia2* that shows anticlockwise helical growth in trichomes, roots and petioles, in correlation to anticlockwise coiling of approximately 10 per cent of the mutant single cells in suspension. This phenotype was linked to an oblique arrangement of the cortical microtubules, which are known to align the cellulose microfibrils [37]. The new coiling principle that we describe may explain this phenomenon as well as hygroscopic movement in other helicoidal cells that have not yet been identified.

## 5. MATERIAL AND METHODS

Wild mature *E. gruinum* dispersal units were collected in the hills of Nes-Tziona, Israel, on 1 May 2009 and kept at ambient conditions. *Erodium gruinum* was germinated according to the procedure described before [31], and dispersal units were continuously collected from the mature plants.

### 5.1. Preparation of cross sections

Mature *E. gruinum* awns were embedded in polyethylene glycol (PEG) 2000 MW as described elsewhere [38]. Cross sections (10 μm thick) from the coiling region were cut on a rotary microtome (LEICA RM2255, Germany), and then placed in water to remove the PEG. The washed cross sections were placed on a glass slide with a drop of water, and sealed with a coverslip to prevent evaporation of water during the measurement.

### *5.2. Scanning electron microscopy*

Two sets of samples from the coiling region of mature awns were measured. In the first one, samples were broken by hand, whereas in the second one, cells were separated using fine tweezers and syringe needles. Both sets were prepared by critical point drying, mounted on aluminium stubs and sputter-coated with gold–palladium. Samples were examined in the environmental scanning electron microscope, XL 30 ESEM FEG (FEI): first set at 5 kV using high vacuum mode, 9.5 mm working distance and second set at 8 kV, using high vacuum mode and 19 mm working distance.

### *5.3. Cryo-scanning electron microscopy*

Wet samples of the coiling region of the *E. gruinum* awn, in which cells were separated using fine tweezers and syringe needles, were mounted on metal holders. The samples were plunged in liquid nitrogen, transferred to a BAF 60 (Bal-Tec, Liechtenstein, Germany) freeze fracture device kept at $-120^{\circ}$C, and rotary coated with 6 nm platinum/carbon coating at variable angle (15–90°). The coated samples were transferred to an Ultra 55 SEM (Zeiss, Germany) equipped with a cryo-stage (Bal-Tec) using a VCT 100 (Bal-Tec) vacuum-cryo transfer device. Working distance was 9 mm, and the accelerating voltage was 2.5 kV.

### *5.4. Small-angle X-ray scattering*

Scattering experiments were performed using CuK$\alpha$ radiation ($\lambda = 0.154$ nm) from a Rigaku RA-MicroMax 007 HF X-ray generator operated at a power rating of up to 1.2 kW. The beam size at the sample position was $0.7 \times 0.7$ mm, as defined by a set of two scatterless slits [39]. The scattered beam went through a flight path filled with He, and reached a Mar345 image plate detector.

The inner and outer faces of the coiling region of the *E. gruinum* awn were separated using a razor blade. Sections from the wet inner face were inserted into 1.5 mm quartz capillaries, to which 10 µl distilled water were added to maintain their wet state. The capillaries were flame-sealed and mounted vertically in a perpendicular orientation to the X-ray beam. Experiments were carried out at room temperature. Each sample was checked before and after the experiment to verify that no fluid was lost during the time of exposure (approx. 1 h). The sample distance to the detector was 1841.3 mm, calibrated using silver behenate. Background correction was verified by measuring the scattering of a capillary filled with distilled water and correcting for sample absorption. Integration of the scattering density was performed using Fit2d software. Scattered intensity was plotted as a function of the scattering vector $q = (4\pi/\lambda) \cdot \sin\,\theta$, where $\lambda$ is the X-ray wavelength and $\theta$ is half the angle between the incident and scattered wavevectors.

### *5.5. Sponge models*

Long rectangular cylinders of polyurethane foam, of about $1.5 \times 1.5$ cm cross section, were woven with a cotton thread to create a normal and sheared helix. The thread was tightened in order to simulate an expanding matrix encased in a sheared helical scaffold.

We thank Eran Sharon, Kalman Schulgasser and Asaph Aharoni for their support and fruitful discussions, and Markus Rüggeberg for his help in creating the awn movie. The electron microscopy studies were conducted at the Irving and Cherna Moskowitz Centre for Nano and Bio-Nano Imaging at the Weizmann Institute of Science. This work was supported by The Israel Science Foundation grant 598/10.

## REFERENCES

1 Fowler, N. L. 1988 What is a safe site? Neighbor, litter, germination date, and patch effects. *Ecology* **69**, 947–961. (doi:10.2307/1941250)
2 Van der Pijl, L. 1982 *Principles of dispersal in higher plants,* 3rd edn. New York, NY: Springer.
3 Fahn, A. & Werker, E. 1972 Anatomical mechanisms of seed dispersal. In *Seed biology* (ed. T. T. Kozlowski), pp. 151–221. New York, NY: Academic Press.
4 Harper, J. L., Lovell, P. H. & Moore, K. G. 1970 The shapes and sizes of seeds. *Annu. Rev. Ecol. Syst.* **1**, 327–356. (doi:10.1146/annurev.es.01.110170.001551)
5 Elbaum, R., Zaltzman, L., Burgert, I. & Fratzl, P. 2007 The role of wheat awns in the seed dispersal unit. *Science* **316**, 884–886. (doi:10.1126/science.1140097)
6 Reyssat, E. & Mahadevan, L. 2009 Hygromorphs: from pine cones to biomimetic bilayers. *J. R. Soc. Interface* **6**, 951–957. (doi:10.1098/rsif.2009.0184)
7 Lacey, E. P., Kaufman, P. B. & Dayanandan, P. 1983 The anatomical basis for hygroscopic movement in primary rays of *Daucus carota* ssp. *carota* (Apiaceae). *Bot. Gaz.* **144**, 371–375. (doi:10.1086/337385)
8 Simpson, M. G. 2006 *Plant systematics*. Amsterdam, The Netherlands: Elsevier Academic Press.
9 Ueno, J. 1975 Moving mechanism of elater in the spore of *Equisetum arvense*. *Jpn. J. Palynol.* **15**, 67–71. (In Japanese).
10 Simpson, M. G. 2006 *Plant systematics*. Amsterdam, The Netherlands: Elsevier Academic Press.
11 Burgert, I. & Fratzl, P. 2009 Actuation systems in plants as prototypes for bioinspired devices. *Phil. Trans. R. Soc. A* **367**, 1541–1557. (doi:10.1098/rsta.2009.0003)
12 Fahn, A. 1990 *Plant anatomy*, 4th edn. Oxford, UK: Pergamon Press.
13 Fry, S. C. 1999 Plant cell walls. In *Encyclopedia of life sciences*. London, UK: John Wiley & Sons, Nature Publishing Group. (doi:10.1038/npg.els.0001682)
14 Niklas, K. 1992 *Plant biomechanics: an engineering approach to plant form and function*. Chicago, IL: University of Chicago Press.
15 Fratzl, P. & Barth, F. G. 2009 Biomaterial systems for mechanosensing and actuation. *Nature* **462**, 442–448. (doi:10.1038/nature08603)
16 Fratzl, P., Elbaum, R. & Burgert, I. 2008 Cellulose fibrils direct plant organ movements. *Faraday Discuss.* **139**, 275–282. (doi:10.1039/b716663j)
17 Uphof, J. C. T. 1924 Hygrochastic movements in floral bracts of *Ammobium*, *Acroclinium*, *Rhodanthe*, and *Helichrysum*. *Am. J. Bot.* **11**, 159–163. (doi:10.2307/2435536)
18 Fahn, A. & Zohary, M. 1955 On the pericarpial structure of the legumen, its evolution and relation to dehiscence. *Phytomorphology* **5**, 99–111.
19 Dawson, C., Vincent, J. F. V. & Rocca, A. 1997 How pine cones open. *Nature* **390**, 668. (doi:10.1038/37745)
20 Witztum, A. & Schulgasser, K. 1995 The mechanics of seed expulsion in Acanthaceae. *J. Theor. Biol.* **176**, 531–542. (doi:10.1006/jtbi.1995.0219)

21 Chen, Z., Majidi, C., Srolovitz, D. J. & Haataja, M. 2011 Tunable helical ribbons. *App. Phys. Lett.* **98**, 011906. (doi:10.1063/1.3530441)
22 Evangelista, D., Hotton, S. & Dumais, D. 2011 The mechanics of explosive dispersal and self-burial in the seeds of the filaree, *Erodium cicutarium* (Geraniaceae). *J. Exp. Biol.* **214**, 521–529. (doi:10.1242/jeb.050567)
23 Stamp, N. E. 1989 Efficacy of explosive versus hygroscopic seed dispersal by an annual grassland species. *Am. J. Bot.* **76**, 555–561. (doi:10.2307/2444350)
24 Stamp, N. E. 1984 Self-burial behaviour of *Erodium cicutarium* seeds. *J. Ecol.* **72**, 611–620. (doi:10.2307/2260070)
25 Alsberg, C. L. 1938 Structure of the starch granule. *Plant Physiol.* **13**, 295–330. (doi:10.1104/pp.13.2.295)
26 Reiterer, A., Lichtenegger, H., Fratzl, P. & Stanzl-Tschegg, S. E. 2001 Deformation and energy absorption of wood cell walls with different nanostructure under tensile loading. *J. Mater. Sci.* **36**, 4681–4686. (doi:10.1023/A:1017906400924)
27 Nadler, M. *et al.* 2011 Following the structural changes during zinc-induced crystallization of charged membranes using time-resolved solution X-ray scattering. *Soft Matter* **7**, 1512–1523. (doi:10.1039/c0sm00824a)
28 Cave, I. D. 1968 The anisotropic elasticity of the plant cell wall. *Wood Sci. Technol.* **2**, 268–278. (doi:10.1007/BF00350273)
29 Burgert, I., Frühmann, K., Keckes, J., Fratzl, P. & Stanzl-Tschegg, S. 2005 Properties of chemically and mechanically isolated fibres of spruce (*Picea abies* [L.] Karst.). Part 2: twisting phenomena. *Holzforschung* **59**, 247–251. (doi:10.1515/HF.2005.039)
30 Lichtenegger, H., Müller, M., Paris, O., Riekel, C. & Fratzl, P. 1999 Imaging of the helical arrangement of cellulose fibrils in wood by synchrotron X-ray microdiffraction. *J. Appl. Crystallogr.* **32**, 1127–1133. (doi:10.1107/S0021889899010961)
31 Young, J. A. E., Kay, R. A. & Burgess, L. 1974 Dispersal and germination dynamics of broadleaf filaree, *Erodium botrys* (cav.) bertol. *Agron. J.* **67**, 54–57. (doi:10.2134/agronj1975.00021962006700010014x)
32 Zohary, M. 1937 Die verbreitungsökologischen Verhältnisse der pflanzen Paläestinas. *Beih. Bot. Zentbl. A* **56**, 1–155.
33 Ghafouri, R. & Bruinsma, R. 2005 Helicoid to spiral ribbon transition. *Phys. Rev. Lett.* **94**, 138101. (doi:10.1103/PhysRevLett.94.138101)
34 Gray, D. G. 1989 Chirality and curl of paper sheets. *J. Pulp Paper Sci.* **15**, J105–J109.
35 Elbaum, R., Gorb, S. & Fratzl, P. 2008 Structures in the cell wall that enable hygroscopic movement of wheat awns. *J. Struct. Biol.* **164**, 101–107. (doi:10.1016/j.jsb.2008.06.008)
36 Probine, M. C. 1963 Cell growth and the structure and mechanical properties of the wall in internodal cells of *Nitella opaca*: III. Spiral growth and cell wall structure. *J. Exp. Bot.* **14**, 101–113. (doi:10.1093/jxb/14.1.101)
37 Buschmann, H., Hauptmann, M., Niessing, D., Lloyd, C. & Schaffner, A. 2009 Helical growth of the *Arabidopsis* mutant tortifolia2 does not depend on cell division patterns but involves handed twisting of isolated cells. *Plant Cell* **21**, 2090–2106. (doi:10.1105/tpc.108.061242)
38 Rüggeberg, M., Speck, T., Paris, O., Lapierre, C., Pollet, B., Koch, G. & Burgert, I. 2008 Stiffness gradients in vascular bundles of the palm *Washingtonia robusta*. *Proc. R. Soc. B* **275**, 2221–2229. (doi:10.1098/rspb.2008.0531)
39 Li, Y., Beck, R., Huang, T., Choi, M. C. & Divinagracia, M. 2008 Scatterless hybrid metal-single-crystal slit for small-angle X-ray scattering and high-resolution X-ray diffraction. *J. Appl. Crystallogr.* **41**, 1134–1139. (doi:10.1107/S0021889808031129)